A Geometric Approach to Strapdown Magnetometer Calibration in Sensor Frame

J.F. Vasconcelos, *Member, IEEE,* G. Elkaim, *Member, IEEE,* C. Silvestre *Member, IEEE,*
P. Oliveira *Member, IEEE,* and B. Cardeira *Member, IEEE*

Abstract

In this work a new algorithm is derived for the onboard calibration of three-axis strapdown magnetometers. The proposed calibration method is written in the sensor frame, and compensates for the combined effect of all linear time-invariant distortions, namely soft iron, hard iron, sensor non-orthogonality, bias, among others. A Maximum Likelihood Estimator (MLE) is formulated to iteratively find the optimal calibration parameters that best fit to the onboard sensor readings, without requiring external attitude references. It is shown that the proposed calibration technique is equivalent to the estimation of a rotation, scaling and translation transformation, and that the sensor alignment matrix is given by the solution of the orthogonal Procrustes problem. Good initial conditions for the iterative algorithm are obtained by a suboptimal batch least squares computation. Simulation and experimental results with low-cost sensors data are presented and discussed, supporting the application of the algorithm to autonomous vehicles and other robotic platforms.

Index Terms

Calibration; Magnetic fields; Maximum likelihood estimators; Least-squares algorithm.

I. Introduction

Magnetometers are a key aiding sensor for attitude estimation in low-cost, high performance navigation systems [1], [2], [3], [4], with widespread application to autonomous air, ground and ocean vehicles. These inexpensive, low power sensors allow for accurate attitude estimates by comparing the magnetic field vector observation in body frame coordinates with the vector representation in Earth frame coordinates, available from geomagnetic charts and software [5]. In conjunction with vector observations provided by other sensors such as star trackers or pendulums, the magnetometer triad yields complete 3-DOF attitude estimation [3], [6].

The magnetic field reading distortions occur in the presence of ferromagnetic elements found in the vicinity of the sensor and due to devices mounted in the vehicle's structure. Other sources of disturbances are associated with technological limitations in sensor manufacturing and installation. A comprehensive description of the magnetic compass theory can be found in [7].

Magnetometer calibration is an old problem in ship navigation and many calibration techniques have been presented in the literature. The classic compass swinging calibration technique proposed in [8] is a heading calibration algorithm that computes scalar parameters using a least squares algorithm. The major shortcoming of this approach is the necessity of an external heading information [9], which is a strong requirement in many applications. A tutorial work using a similar but more sound mathematical derivation is found in [7]. This book addresses the fundamentals of magnetic compass theory and presents a methodology to calibrate the soft and hard iron parameters in heading and pitch, resorting only to the magnetic compass data. However, the calibration algorithm is derived by means of successive approximations and is formulated in a deterministic fashion that does not exploit the data of multiple compass readings.

In recent literature, advanced magnetometer calibration algorithms have been proposed to tackle distortions such as bias, hard iron, soft iron and non-orthogonality directly in the sensor space, with no external attitude references and using optimality criteria. The batch least squares calibration algorithm derived in [10], [9] accounts for non-orthogonality, scaling and bias errors. A nonlinear, two-step estimator provides the initial conditions using a nonlinear change of variables to cast the calibration in a pseudo-linear least squares form. The obtained estimate of the calibration parameters is then iteratively processed by a linearized least squares batch algorithm.

The TWOSTEP batch method proposed in [11] is based on the observations of the differences between the actual and the measured unit vector, denoted as scalar-checking. In the first step of the algorithm, the centering approximation derived in [12] produces a good initial guess of the calibration parameters, by rewriting the calibration problem in a linear least squares form. In a second step, a batch Gauss-Newton method is adopted to iteratively estimate the bias, scaling and non-orthogonality parameters. In related work, [13] derives recursive algorithms for magnetometer calibration based on the centering approximation and on nonlinear Kalman filtering techniques.

J.F. Vasconcelos, C. Silvestre, P. Oliveira and B.Cardeira are with the Institute for Systems and Robotics (ISR), Instituto Superior Técnico, Lisbon, Portugal. E-mails: {jfvasconcelos, cjs, pjcro, bcardeira}@isr.ist.utl.pt Tel: (+351) 21-8418054, Fax: (+351) 21-8418291.

G. Elkaim is with the Department of Computer Engineering, University of California Santa Cruz, 1156 High St., Santa Cruz, CA, 95064. E-mail: elkaim@soe.ucsc.edu

Magnetic errors such as soft iron, hard iron, scaling, bias and non-orthogonality are modeled separately in [10]. Although additional magnetic transformations can be modeled, it is known that some sensor errors are compensated by an equivalent effect, e.g. the hard iron and sensor biases are grouped together in [9]. Therefore, the calibration procedure should address the estimation of the joint effect of the sensor errors, as opposed to estimating each effect separately.

In this work, the magnetometer reading error model is discussed and cast in a error formulation which accounts for the combined effect of all linear time-invariant magnetic transformations. A rigorous geometric formulation simplifies the problem of compensating for the modeled and unmodeled magnetometer errors to that of the estimation of parameters lying on an ellipsoid manifold. A complete methodology to calibrate the magnetometer is detailed, and a Maximum Likelihood Estimator (MLE) allows for the formulation of the calibration problem as the optimization of the sensor readings likelihood.

The sensor calibration problem is naturally formulated in the sensor frame. The calibration parameters are estimated using the magnetometer readings, and without resorting to external information or models about the magnetic field. In addition, a closed form solution for the sensor alignment is also presented, based on the well known solution to the orthogonal Procrustes problem [14].

The proposed calibration methodology is assessed both in simulation and using experimental data. Because the calibration parameters are influenced by the magnetic characteristics of the payload, the geomagnetic profile of the terrain and diverse vehicle operating conditions, the online calibration of the magnetometers is analyzed. The calibration parameters are estimated for magnetometer data collected in ring shaped sets, corresponding to yaw and pitch maneuvers that are feasible for most land, air and ocean vehicles. Simulation and experimental results show that the algorithm performs a computationally fast calibration with accurate parameter estimation.

To the best of the authors' knowledge, this work is an original rigorous derivation of a calibration algorithm using a comprehensive model of the sensor readings in $\mathbb{R}^3$, that clarifies and exploits the geometric locus of the magnetometer readings, given by an ellipsoid manifold. It is also shown that the calibration and alignment procedures are distinct.

This paper is organized as follows. In Section II, a unified magnetometer error parametrization is derived and formulated. It is shown that the calibration parameters describe an ellipsoid surface and that the calibration and alignment problems are distinct. A MLE formulation is proposed to calculate the optimal generic calibration parameters and an algorithm to provide good initial conditions is presented. Also, a closed form solution for the magnetometer alignment problem is obtained. Simulation and experimental results obtained with a low-cost magnetometer triad are presented and discussed in Section III. Finally, Section IV draws concluding remarks and comments on future work.

II. Magnetometer Calibration and Alignment

In this section, an equivalent parametrization of the magnetometer errors is derived. The main sources of magnetic distortion and bias are characterized, to yield a comprehensive structured model of the magnetometer readings. Using this detailed parametrization as a motivation, the magnetometer calibration problem is recast, without loss of generality, into a unified transformation parametrized by a rotation $\mathcal{R}$, a scaling $\mathbf{S}$, and an offset $\mathbf{b}$. Consequently, it is shown that for all linear transformations of the magnetic field, such as soft and hard iron, non-orthogonality, scaling factor and sensor bias, the magnetometer readings will always lie on an ellipsoid manifold.

A Maximum Likelihood Estimator formulation is proposed to find the optimal calibration parameters which maximize the likelihood of the sensor readings. The proposed calibration algorithm is derived in the sensor frame and does not require any specific information about the magnetic field's magnitude and body frame coordinates. This fact allows for magnetometer calibration without external aiding references. Also, a closed form optimal algorithm to align the magnetometer and body coordinate frames is obtained from the solution to the orthogonal Procrustes problem.

A. Magnetometer Errors Characterization

The magnetometer readings are distorted by the presence of ferromagnetic elements in the vicinity of the sensor, the interference between the magnetic field and the vehicle structure, local permanently magnetized materials, and by sensor technological limitations.

Hard Iron / Soft Iron: The hard iron bias, denoted as $\mathbf{b}_{HI}$, is the combined result of the permanent magnets inherent to the vehicle's structure, as well as other elements installed in the vehicle, and it is constant in the vehicle's coordinate frame.

Soft iron effects are generated by the interaction of an external magnetic field with the ferromagnetic materials in the vicinity of the sensor. The resulting magnetic field depends on the magnitude and direction of the applied magnetic field with respect to the soft iron material, producing

$$\mathbf{h}_{SI} = \mathbf{C}_{SI}\,{}^{B}_{E}\mathbf{R}\,{}^{E}\mathbf{h} \tag{1}$$

where $\mathbf{C}_{SI} \in \mathrm{M}(3)$ is the soft iron transformation matrix, ${}^{E}_{B}\mathbf{R}$ is the rotation matrix from body to Earth coordinate frames, ${}^{B}_{E}\mathbf{R} := {}^{E}_{B}\mathbf{R}'$, ${}^{E}\mathbf{h}$ is the Earth magnetic field, $\mathrm{M}(n,m)$ denotes the set of $n \times m$ matrices with real entries and $\mathrm{M}(n) := \mathrm{M}(n,n)$. As described in [7, chapter XI], the combined hard and soft iron effects are given by $\mathbf{h}_{SI+HI} = \mathbf{h}_{SI} + \mathbf{b}_{HI}$. The linearization of the ferromagnetic effects (1) yields the well known heading error $\delta\psi$ model [7], [9] adopted in compass swinging calibration,

which ignores the harmonics above 2ψ. The formulation (1), adopted in this paper, yields a rigorous approach to the simultaneous estimation of the hard and soft iron effects.

Non-orthogonality: The non-orthogonality of the sensors can be described as a transformation of vector space basis, parametrized by [15]

$$\mathbf{C}_{NO} = \begin{bmatrix} 1 & 0 & 0 \\ \sin(\psi) & \cos(\psi) & 0 \\ -\sin(\theta) & \cos(\theta)\sin(\phi) & \cos(\theta)\cos(\phi) \end{bmatrix} \tag{2}$$

where (ψ, θ, ϕ) are Yaw, Pitch and Roll Euler angles, respectively.

Scaling and Bias: The null-shift or offset of the sensor readings is modeled as a constant vector $\mathbf{b}_M \in \mathbb{R}^3$. The transduction from the electrical output of the sensor to the measured quantity is formulated as a scaling matrix $\mathbf{S}_M \in \mathrm{D}^+(3)$, where $\mathrm{D}(n)$ denotes the set of $n \times n$ diagonal matrices with real entries and $\mathrm{D}^+(n) = \{\mathbf{S} \in \mathrm{D}(n) : \mathbf{S} > 0\}$.

Wideband noise: The disturbing noise is assumed wideband compared with the bandwidth of the system, yielding uncorrelated sensor sampled noise.

Alignment with the body frame: The formulation of the proposed algorithm in the sensor frame allows for sensor calibration without determination of the alignment of the sensor with respect to a reference frame. An alignment procedure of the sensor triad is proposed in this paper for the sake of completeness.

Other effects: Generic and more complex effects related to sensor-specific characteristics and to the magnetic distortion are difficult to model accurately. The proposed calibration algorithm compensates for the combined influence of all linear time-invariant transformations that distort the magnetic field, which are estimated in the form of an equivalent linear transformation.

B. Magnetometer Error Parametrization

In this section, an equivalent error model for the magnetometer readings is formulated. First, the estimation problem of the non-ideal magnetic effects described in Section II-A is recast, without loss of generality, as the problem of estimating an affine linear transformation. Second, it is shown that the linear transformation is equivalent to a single rotation, scaling and translation transformation. In other words, to calibrate the magnetometer it is sufficient to estimate the center, orientation and radii of the ellipsoid that best fit to the acquired data.

Define a sphere and an ellipsoid as [16]

$$\mathrm{S}(n) = \{\mathbf{x} \in \mathbb{R}^{n+1} : \|\mathbf{x}\|^2 = 1\}, \quad \mathrm{L}(n) = \{\mathbf{x} \in \mathbb{R}^{n+1} : \|\mathbf{S}\mathcal{R}'\mathbf{x}\|^2 = 1\} \tag{3}$$

where $\mathbf{S} \in \mathrm{D}^+(n+1)$ and $\mathcal{R} \in \mathrm{SO}(n+1)$ describe the radii and orientation of the ellipsoid, respectively, and $\mathrm{SO}(n) = \{\mathcal{R} \in \mathrm{O}(n) : \det(\mathcal{R}) = 1\}$, $\mathrm{O}(n) = \{\mathbf{U} \in \mathrm{M}(n) : \mathbf{U}\mathbf{U}' = \mathbf{I}_{n\times n}\}$. The three-axis magnetometer reading is given by the Earth's magnetic field ${}^E\mathbf{h}$ affected by the magnetic distortions and errors, yielding

$$\mathbf{h}_{r\,i} = \mathbf{S}_M\mathbf{C}_{NO}(\mathbf{C}_{SI}\,{}^B_E\mathbf{R}_i\,{}^E\mathbf{h} + \mathbf{b}_{HI}) + \mathbf{b}_M + \mathbf{n}_{m\,i} \tag{4}$$

where $\mathbf{h}_r$ is the magnetometer reading in the (non-orthogonal) magnetometer coordinate frame, $\mathbf{n}_m \in \mathbb{R}^3$ is the Gaussian wideband noise, $\mathbf{S}_M$, $\mathbf{C}_{NO}$, $\mathbf{C}_{SI}$, $\mathbf{b}_{HI}$ and $\mathbf{b}_M$ are the magnetic distortions described in Section II-A, and $i = 1, \ldots, n$ denotes the index of the reading.

Without loss of generality, the magnetometer reading can be described by

$$\mathbf{h}_{r\,i} = \mathbf{C}\,{}^B\mathbf{h}_i + \mathbf{b} + \mathbf{n}_{m\,i} \tag{5}$$

where $\mathbf{C} = \mathbf{S}_M\mathbf{C}_{NO}\mathbf{C}_{SI}$, $\mathbf{b} = \mathbf{S}_M\mathbf{C}_{NO}\mathbf{b}_{HI} + \mathbf{b}_M$, ${}^B\mathbf{h}_i = {}^B_E\mathbf{R}_i\,{}^E\mathbf{h}$, ${}^B\mathbf{h}_i \in \mathrm{S}(2)$ is the magnetic field in body coordinate frame. In particular, $\mathbf{C} \in \mathrm{M}(3)$ and $\mathbf{b} \in \mathbb{R}^3$ are unconstrained, so unmodeled linear time-invariant magnetic errors and distortions are also taken into account.

Given that the points ${}^B\mathbf{h}_i$ are contained in the sphere, straightforward application of the Singular Value Decomposition (SVD) [16] shows that the magnetometer readings $\mathbf{h}_{r\,i}$ lie on an ellipsoid manifold, as illustrated in the example of Fig. 1 and summarized in the following theorem. The proof is presented for the sake of clarity.

Theorem 1 ([16]): Let $c : \mathbb{R}^n \to \mathbb{R}^n, c(\mathbf{x}) = \mathbf{C}\mathbf{x}$ be a linear transformation where $\mathbf{C} \in \mathrm{M}(n)$ is full rank. Then $c(\mathbf{x})$ is a bijective transformation between the sphere and an ellipsoid in $\mathbb{R}^n$, i.e. there is an ellipsoid $\mathrm{L}(n-1)$ such that the transformation $c|_{\mathrm{S}} : \mathrm{S}(n-1) \to \mathrm{L}(n-1), \quad c|_{\mathrm{S}}(\mathbf{x}) = \mathbf{C}\mathbf{x}$ is bijective.

Proof: Let the SVD decomposition $\mathbf{C} = \mathbf{U}\mathbf{\Sigma}\mathbf{V}'$, where $\mathbf{U}, \mathbf{V} \in \mathrm{O}(n)$ and $\mathbf{\Sigma} \in \mathrm{D}^+(n)$. Define the matrices $\mathcal{R}_L := \mathbf{U}\mathbf{J}, \mathbf{S}_L := \mathbf{\Sigma}, \mathbf{V}_L := \mathbf{V}\mathbf{J}, \mathbf{J} := \begin{bmatrix} \det(\mathbf{U}) & \mathbf{0} \\ \mathbf{0} & \mathbf{I}_{n-1\times n-1} \end{bmatrix}$, which describe a modified SVD decomposition with at least one special orthogonal matrix $\mathbf{C} = \mathcal{R}_L\mathbf{S}_L\mathbf{V}_L'$ where $\mathcal{R}_L \in \mathrm{SO}(n)$, $\mathbf{S}_L \in \mathrm{D}^+(n)$ and $\mathbf{V}_L \in \mathrm{O}(n)$. The transformation $c(\mathbf{x})$ applied to the sphere is given by

$$c|_S(\mathbf{x}) := \mathcal{R}_L\mathbf{S}_L\mathbf{y} \tag{6}$$

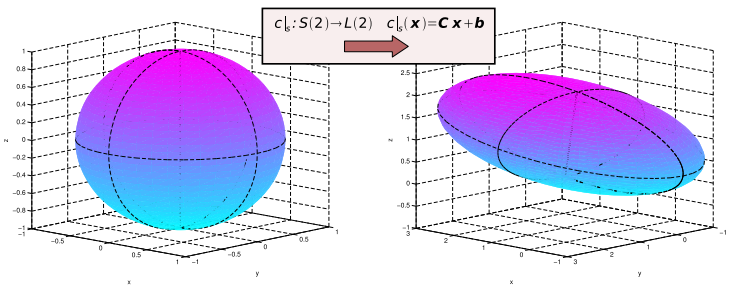

Fig. 1. Affine transformation of a two dimensional sphere

where $\mathbf{y} := \mathbf{V}_L'\mathbf{x}$ verifies $\|\mathbf{y}\|^2 = 1$. Choosing the ellipsoid $\mathrm{L}(n-1) = \{\mathbf{x} \in \mathbb{R}^n : \|\mathbf{S}_L^{-1}\mathcal{R}_L'\mathbf{x}\|^2 = 1\}$ then $c|_S(\mathbf{x}) \in \mathrm{L}(n-1)$. The function (6) is injective because $\mathcal{R}_L\mathbf{S}_L$ is invertible. To see that it is surjective, given any $\mathbf{z} \in \mathrm{L}(n-1)$, the point $\mathbf{y} = \mathbf{S}_L^{-1}\mathcal{R}_L'\mathbf{z} \in \mathrm{S}(n-1)$ satisfies $c(\mathbf{y}) = \mathbf{z}$. ■

Corollary 1: Let $\mathbf{C} \in \mathrm{M}(n)$ be a full rank matrix and let the SVD decomposition of $\mathbf{C}$ be given by $\mathbf{C} = \mathcal{R}_L\mathbf{S}_L\mathbf{V}_L'$ where $\mathcal{R}_L \in \mathrm{SO}(n)$, $\mathbf{S}_L \in \mathrm{D}^+(n)$ and $\mathbf{V}_L \in \mathrm{O}(n)$. The ellipsoid described by $c|_S$ is spanned by the bijective transformation $l : \mathrm{S}(n-1) \to \mathrm{L}(n-1), \quad l(\mathbf{x}) = \mathcal{R}_L\mathbf{S}_L\mathbf{x}$.

Theorem 1 implies that the magnetic field readings $\mathbf{h}_{r\,i}$ derived in (5) lie on the surface of an ellipsoid centered on $\mathbf{b}$, referred to as sensor ellipsoid. Corollary 1 states that the sensor ellipsoid centered at $\mathbf{b}$ is fully characterized the rotation $\mathcal{R}_L$ and scaling $\mathbf{S}_L$ matrices.

Define ${}^C\mathbf{h}_i := \mathbf{V}_L'\,{}^B\mathbf{h}_i, {}^C\mathbf{h}_i \in \mathrm{S}(2)$ where the coordinate frame $\{C\}$ is obtained by the orthogonal transformation $\mathbf{V}_L'$ of $\{B\}$, i.e. by the alignment matrix $\mathbf{V}_L$. The equivalent model for the magnetometer readings (5) is described by

$$\mathbf{h}_{r\,i} = \mathcal{R}_L\mathbf{S}_L\,{}^C\mathbf{h}_i + \mathbf{b} + \mathbf{n}_{m\,i} \tag{7}$$

Clearly, the calibration process is equivalent to the estimation of the ellipsoid's parameters $\mathbf{b}$, $\mathcal{R}_L$ and $\mathbf{S}_L$. As expected, the alignment matrix $\mathbf{V}_L$ is not observable in the calibration process given that ${}^C\mathbf{h}_i$ and ${}^B\mathbf{h}_i$ are not measured.

The sensor description (7) is a function of the calibration parameters $(\mathcal{R}_L, \mathbf{S}_L, \mathbf{b})$ lying on the manifold $\mathrm{SO}(3)\times\mathrm{D}^+(3)\times\mathbb{R}^3$. Optimization tools on Riemannian manifolds are required to solve for the calibration parameters directly on $\mathrm{SO}(3)\times\mathrm{D}^+(3)\times\mathbb{R}^3$, see [17], [18] for a comprehensive introduction to the subject. Fortunately, an equivalent calibration can be performed in the Euclidean space $\mathrm{M}(3)$ by estimating $\mathbf{C}$ directly, but where the fact that the alignment matrix $\mathbf{V}_L$ cannot be determined must be considered.

The sensor calibration and alignment algorithm is structured as follows. In the *calibration* step, the parameters $\mathcal{R}_L$, $\mathbf{S}_L$ and $\mathbf{b}$ are estimated, using a Maximum Likelihood Estimator formulated on $\mathrm{M}(3)$. In the *alignment* step, the determination of the orthogonal transformation $\mathbf{V}_L$ is obtained from a closed form optimal algorithm using vector readings in $\{C\}$ and $\{B\}$ frames.

C. Magnetometer Calibration

The calibration parameters are computed using a Maximum Likelihood Estimator. An intermediate estimator is formulated on the manifold $\Theta := \mathrm{SO}(3) \times \mathrm{D}^+(3) \times \mathbb{R}^3$ to evidence that the sensor alignment cannot be determined by a calibration algorithm written in the sensor frame. However, the use of classical optimization tools in Euclidean spaces is allowed for by writing an equivalent estimator formulation on $\mathrm{M}(3)$.

Assuming that the noise on the magnetometer readings is a zero mean Gaussian process with variance $\sigma_{m\,i}^2$, the probability density function (p.d.f.) of each $\mathbf{h}_{r\,i}$ is also Gaussian

$$\mathbf{n}_{m\,i} \sim \mathcal{N}(0, \sigma_{m\,i}^2\mathbf{I}) \Rightarrow \mathbf{h}_{r\,i} \sim \mathcal{N}(\mathcal{R}_L\mathbf{S}_L\,{}^C\mathbf{h}_i + \mathbf{b}, \sigma_{m\,i}^2\mathbf{I})$$

The MLE finds the parameters that maximize the conditional p.d.f. of each sensor reading given the optimization parameters [19]. The resulting minimization problem of the weighted log-likelihood function is described by

$$\min_{\substack{(\mathcal{R}_L,\mathbf{S}_L,\mathbf{b})\in\Theta \\ {}^C\mathbf{h}_i\in\mathrm{S}(2), i=1,\ldots,n}} \sum_{i=1}^{n} \left(\frac{\|(\mathbf{h}_{r\,i} - \mathbf{b}) - \mathcal{R}_L\mathbf{S}_L\,{}^C\mathbf{h}_i\|}{\sigma_{m\,i}} \right)^2 \tag{8}$$

The minimum of (8) is computed iteratively by gradient or Newton-like methods on manifolds [17], [18]. Note that solving the minimization problem (8) implies estimating n auxiliary magnetic field vectors ${}^C\mathbf{h}_i$, and the dimension of the search space is $(2n + \dim\Theta)$ whereas the dimension of the calibration parameters space is $\dim\Theta = \dim\mathrm{SO}(3) + \dim\mathrm{D}^+(3) + \dim\mathbb{R}^3 = 9$.

The minimization problem (8) finds the ellipsoid points $(\mathcal{R}_L\mathbf{S}_L\,{}^C\mathbf{h}_i)$ that best fit the sensor readings $(\mathbf{h}_{r\,i} - \mathbf{b})$. Intuitively, the minimization problem can be rewritten to find the sphere points ${}^C\mathbf{h}_i$ that best fit to the pullback of the ellipsoid to the

sphere $(\mathbf{S}_L^{-1}\mathcal{R}'_L(\mathbf{h}_{r\,i}-\mathbf{b}))$, yielding

$$\min_{\substack{(\mathcal{R}_L,\mathbf{S}_L,\mathbf{b})\in\Theta\\ {}^C\mathbf{h}_i\in \mathrm{S}(2), i=1,..,n}} \sum_{i=1}^{n}\left(\frac{\|\mathbf{S}_L^{-1}\mathcal{R}'_L(\mathbf{h}_{r\,i}-\mathbf{b})-{}^C\mathbf{h}_i\|}{\sigma_{m\,i}}\right)^2 \tag{9}$$

The minimization problem (9) is suboptimal with respect to the unified error model (7), but can be rigorously derived using a MLE formulation by assuming that the noise is external to the sensor, as detailed in the Appendix More important, the log-likelihood function (9) can be optimized by searching only in the parameter space Θ.

Proposition 1: The solution $(\mathcal{R}_L^*,\mathbf{S}_L^*,\mathbf{b}^*)$ of (9) also minimizes

$$\min_{(\mathcal{R}_L,\mathbf{S}_L,\mathbf{b})\in\Theta} \sum_{i=1}^{n}\left(\frac{\|\mathbf{S}_L^{-1}\mathcal{R}'_L(\mathbf{h}_{r\,i}-\mathbf{b})\|-1}{\sigma_{m\,i}}\right)^2 \tag{10}$$

Proof: Given $(\mathcal{R}_L^*,\mathbf{S}_L^*,\mathbf{b}^*)$, the optimal ${}^C\mathbf{h}_i^*$ satisfies

$${}^C\mathbf{h}_i^* = \underset{{}^C\mathbf{h}_i\in \mathrm{S}(2)}{\operatorname{argmin}} \|\mathbf{v}_i^* - {}^C\mathbf{h}_i\|^2 \tag{11}$$

where $\mathbf{v}_i^* := \mathbf{S}_L^{*-1}\mathcal{R}_L^{*\prime}(\mathbf{h}_{r\,i}-\mathbf{b}^*)$. The minimization problem (11) corresponds to the projection of $\mathbf{v}_i^*$ on the unit sphere, which has the closed form solution ${}^C\mathbf{h}_i^* = \frac{\mathbf{v}_i^*}{\|\mathbf{v}_i^*\|}$. Therefore, the minimization problem (9) can be written as

$$\min_{(\mathcal{R}_L,\mathbf{S}_L,\mathbf{b})\in\Theta} \sum_{i=1}^{n}\left(\frac{\|\mathbf{S}_L^{-1}\mathcal{R}_L{}'(\mathbf{h}_{r\,i}-\mathbf{b})-\frac{\mathbf{v}_i}{\|\mathbf{v}_i\|}\|}{\sigma_{m\,i}}\right)^2$$

where $\mathbf{v}_i := \mathbf{S}_L^{-1}\mathcal{R}_L{}'(\mathbf{h}_{r\,i}-\mathbf{b})$. Using simple algebraic manipulation produces the likelihood function (10). ■

The minimization problem (10) can be formulated on the Euclidean space, which allows for the use of optimization tools for unconstrained problems [20].

Proposition 2: Let $(\mathbf{T}^*,\mathbf{b}_T^*)$ denote the solution of the unconstrained minimization problem

$$\min_{\mathbf{T}\in \mathrm{M}(3)} \sum_{i=1}^{n}\left(\frac{\|\mathbf{T}(\mathbf{h}_{r\,i}-\mathbf{b}_T)\|-1}{\sigma_{m\,i}}\right)^2 \tag{12}$$

and take the SVD decomposition of $\mathbf{T}^* = \mathbf{U}_T^*\mathbf{S}_T^*\mathbf{V}_T^{*\prime}$, $\mathbf{U}_T\in \mathrm{O}(3)$, $\mathbf{S}_T\in \mathbf{D}^+(3)$, $\mathbf{V}_T\in \mathrm{SO}(3)$. The solution of (10) is given by $\mathbf{R}_L^* = \mathbf{V}_T^*$, $\mathbf{S}_L^* = \mathbf{S}_T^{*\,-1}$, $\mathbf{b}^* = \mathbf{b}_T^*$.

Proof: Using the equality $\|\mathbf{V}_L\mathbf{S}_L^{-1}\mathcal{R}'_L(\mathbf{h}_{r\,i}-\mathbf{b})\| = \|\mathbf{S}_L^{-1}\mathcal{R}'_L(\mathbf{h}_{r\,i}-\mathbf{b})\|$ for any $\mathbf{V}_L\in \mathrm{O}(3)$, and the fact that, by the SVD decomposition, $\mathbf{T} := \mathbf{V}_L\mathbf{S}_L^{-1}\mathcal{R}'_L$ is a generic element of $\mathrm{M}(3)$, produces the desired results. ■

By Proposition 2, the calibration parameters of equation (7) are obtained by solving (12) and decomposing the resulting $\mathbf{T}^*$. Although (12) could be derived using (5), the intermediate derivations (9) and (10) where presented to show that (i) the sensor readings lie on an ellipsoid manifold parametrized by $\mathcal{R}_L$, $\mathbf{S}_L$ and $\mathbf{b}$ (ii) the alignment matrix, represented by $\mathbf{V}_L$ (or $\mathbf{U}_T^*$) cannot be determined in the calibration process, given that there are no body referenced measurements.

In this work, the minimization problem (12) is solved by using the gradient and Newton-descent method for Euclidean spaces [20], and the Armijo rule for the step size determination. The gradient and Hessian of the log-likelihood function are computed analytically and presented in the Appendix .

Given the calibration parameters $(\mathcal{R}_L,\mathbf{S}_L,\mathbf{b})$, an unbiased and unit norm representation of the Earth magnetic field in the calibration frame $\{C\}$ is obtained by algebraic manipulation of (7), resulting in

$${}^C\mathbf{h}_i = \mathbf{S}_L^{-1}\mathcal{R}'_L(\mathbf{h}_{r\,i}-\mathbf{b}). \tag{13}$$

A good initial guess of the scaling and bias calibration parameters is produced by the two-step estimator proposed in [9]. The locus of measurements described by

$$\|{}^E\mathbf{h}\|^2 = \|\mathbf{S}^{-1}(\mathbf{h}_r-\mathbf{b})\|^2$$

is expanded and, by defining a nonlinear change of variables, it is rewritten as pseudo-linear least squares estimation problem

$$H(\mathbf{h}_r)f(\mathbf{b},\mathbf{s}) = b(\mathbf{h}_r) \tag{14}$$

where the matrix $H(\mathbf{h}_r)\in \mathrm{M}(n,6)$ and the vector $b(\mathbf{h}_r)\in\mathbb{R}^n$ are nonlinear functions of the vector readings and the vector of unknowns $f(\mathbf{b},\mathbf{s})\in\mathbb{R}^6$ is a nonlinear function of the calibration parameters. The closed form solution to the least squares problem (14) is found to yield a good first guess of the calibration parameters [15].

In alternative, the algorithm proposed in [21] can produce an initial ellipsoid guess based on the difference-of-squares error criterion using a semidefinite programming (SDP) formulation. However, the SDP algorithm is computationally feasible only for no more than a few hundred samples, whereas the pseudo-linear least squares formulation (14) allows for efficient processing of the several thousands of points contained in the calibration data, which are required in practice.

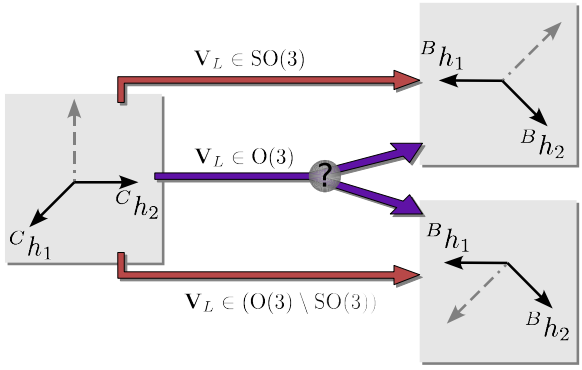

Fig. 2. Alignment estimation ambiguity with two vector readings

D. Magnetometer Alignment

The representation of ${}^{B}\mathbf{h}_i$ in the body frame is necessary in attitude determination algorithms [6]. Although the alignment and calibration procedures are independent, the magnetometer alignment algorithm is detailed for the sake of completeness.

The magnetometer alignment with respect to a reference frame is represented by the orthogonal matrix $\mathbf{V}_L \in \mathrm{O}(3)$ contained in the unified transformation $\mathbf{C}$, see Corollary 1. Given that ${}^{C}\mathbf{h}_i := \mathbf{V}'_L {}^{B}\mathbf{h}_i$, ${}^{C}\mathbf{h}_i \in \mathrm{S}(2)$, the matrix $\mathbf{V}_L$ is computed using the ${}^{C}\mathbf{h}_i$ observations given by the calibrated sensor reading (13), and the ${}^{B}\mathbf{h}_i$ measurements obtained from external information sources, such as heading reference units or external localization systems.

As illustrated in Fig. 2, two vector readings are sufficient to characterize a rigid rotation $\mathbf{V}_L \in \mathrm{SO}(3)$, or a rotation with reflection $\mathbf{V}_L \in (\mathrm{O}(3) \setminus \mathrm{SO}(3))$, but the determination of an orthogonal transformation $\mathbf{V}_L \in \mathrm{O}(3)$ requires at least three linearly independent vectors readings. The well known results for the orthogonal Procrustes problem [14] are adopted to determine $\mathbf{V}_L \in \mathrm{O}(3)$.

Theorem 2 (Orthogonal Procrustes Problem): Take two sets of vector readings in $\{C\}$ and $\{B\}$ coordinate frames, concatenated in the form ${}^{C}\mathbf{X} = \begin{bmatrix} {}^{C}\mathbf{h}_1 & \dots & {}^{C}\mathbf{h}_n \end{bmatrix}$ and ${}^{B}\mathbf{X} = \begin{bmatrix} {}^{B}\mathbf{h}_1 & \dots & {}^{B}\mathbf{h}_n \end{bmatrix}$ where $n \geq 3$. Assume that ${}^{B}\mathbf{X}{}^{C}\mathbf{X}'$ is nonsingular, and denote the corresponding SVD as ${}^{B}\mathbf{X}{}^{C}\mathbf{X}' = \mathbf{U}\mathbf{\Sigma}\mathbf{V}'$, where $\mathbf{U}, \mathbf{V} \in \mathrm{O}(3)$, $\mathbf{\Sigma} \in \mathrm{D}^{+}(3)$. The optimal orthogonal matrix $\mathbf{V}_L^* \in \mathrm{O}(3)$ that minimizes the transformation from $\{B\}$ to $\{C\}$ coordinates frames in least squares sense

$$\min_{\mathbf{V}_L \in \mathrm{O}(3)} \sum_{i=1}^{n} \| {}^{C}\mathbf{h}_i - \mathbf{V}'_L {}^{B}\mathbf{h}_i \|^2$$

is unique and given by $\mathbf{V}'^{*}_L = \mathbf{V}\mathbf{U}'$.

Using (13), the calibrated and aligned magnetic field vector reading is given by

$${}^{B}\mathbf{h}_i = \mathbf{V}_L \mathbf{S}_L^{-1} \mathcal{R}'_L (\mathbf{h}_{r\,i} - \mathbf{b}) \tag{15}$$

Given that the vector magnitude is not relevant for the attitude determination algorithms [6], it is assumed without loss of generality that ${}^{E}\mathbf{h}$ lies on the unit sphere, and the norm scaling factor is thus incorporated in the scaling matrix $\mathbf{S}_L$. Clearly, if $\| {}^{E}\mathbf{h} \| = \alpha, \alpha \neq 1$, the calibrated sensor reading ${}^{B}\mathbf{h}_{i\alpha}$ is given by ${}^{B}\mathbf{h}_{i\alpha} = \alpha {}^{B}\mathbf{h}_i$.

III. Algorithm Implementation and Results

In this section, the proposed calibration algorithm is validated using simulated and experimental data from a triad of low-cost magnetometers.

A. Simulation Results

The calibration algorithm was first analyzed using simulated data. The reference calibration parameters from (4) are

$$\mathbf{S}_M = \mathrm{diag}(1.2, 0.8, 1.3),\ \begin{bmatrix} \psi \\ \theta \\ \phi \end{bmatrix} = \begin{bmatrix} 2.0\,^{\circ} \\ 1.0\,^{\circ} \\ 1.5\,^{\circ} \end{bmatrix},\ \mathbf{b}_{HI} = \begin{bmatrix} -1.2 \\ 0.2 \\ -0.8 \end{bmatrix} \mathrm{G},\ \mathbf{b}_M = \begin{bmatrix} 1.5 \\ 0.4 \\ 2.7 \end{bmatrix} \mathrm{G},\ \mathbf{C}_{SI} = \begin{bmatrix} 0.58 & -0.73 & 0.36 \\ 1.32 & 0.46 & -0.12 \\ -0.26 & 0.44 & 0.53 \end{bmatrix},$$

and the magnetometer noise, described in the sensor space, is a zero mean Gaussian noise with standard deviation $\sigma_m = 5\,\mathrm{mG}$. The likelihood function f is normalized by the number of samples n and the stop condition of the minimization algorithm is $\| \nabla f |_{\mathbf{x}_k} \| < \varepsilon = 10^{-3}$.

In a strapdown sensor architecture, the swinging of the magnetometer triad is constrained by the vehicle's maneuverability and, consequently, only some sections of the ellipsoid can be traced. The magnetic field readings are obtained for two specific cases, illustrated in Fig. 3. In the first case, a ring shaped uniform set of points is obtained for unconstrained Yaw and a Pitch

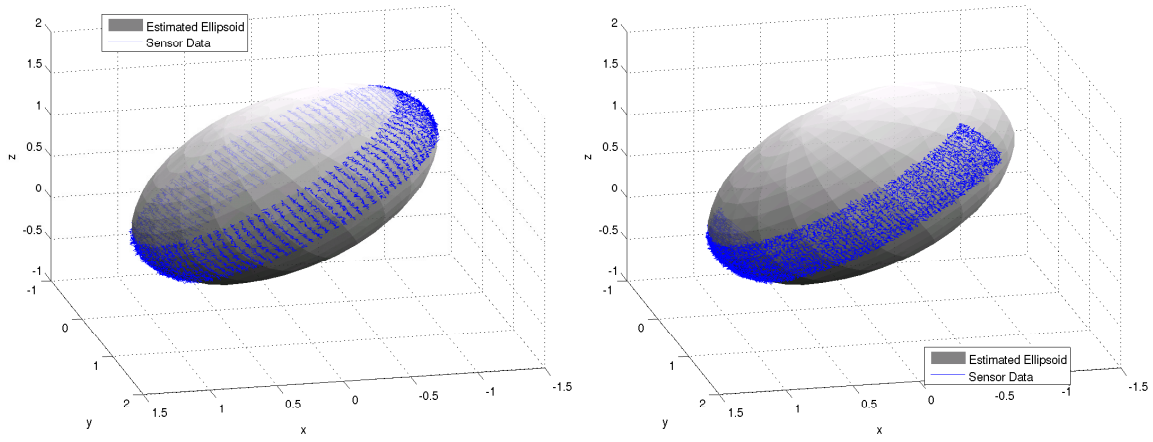

(a) Ring Shaped Data (b) Arch Shaped Data

Fig. 3. Ellipsoid fitting (Simulation Data)

sweep interval of $\theta \in [-20,\ 20]\,^\circ$. Note that the constraint in the Pitch angle can be found in most terrestrial vehicles. In the second case, the ellipsoid's curvature information is reduced by constraining the Yaw to $\psi \in [-90,\ 90]\,^\circ$.

The results of 20 Monte Carlo simulations using 10^4 magnetometer readings are presented in Tables I and II and depicted in Fig. 3. Given the large likelihood cost of the noncalibrated data, denoted by $f(\mathbf{x}_{-1})$, the initial condition draws the cost function into the vicinity of the optimum, and the iterations yield a 20% improvement over the initial guess.

TABLE I
CALIBRATION RESULTS (GRADIENT METHOD)

	$f(\mathbf{x}_{-1})$	$f(\mathbf{x}_0)$	$f(\mathbf{x}^*)$	iterations	θ_e	$\mathbf{s}_e$	$\mathbf{b}_e$
Ring Shaped Data	3.28×10^{-1}	1.17×10^{-4}	9.64×10^{-5}	2246	1.74×10^{-3}	7.61×10^{-3}	3.54×10^{-4}
Arch Shaped Data	4.36×10^{-1}	1.18×10^{-4}	9.62×10^{-5}	1932	1.46×10^{-2}	1.65×10^{-2}	1.74×10^{-2}

TABLE II
CALIBRATION RESULTS (NEWTON METHOD)

	$f(\mathbf{x}_{-1})$	$f(\mathbf{x}_0)$	$f(\mathbf{x}^*)$	iterations	θ_e	$\mathbf{s}_e$	$\mathbf{b}_e$
Ring Shaped Data	3.28×10^{-1}	1.18×10^{-4}	9.64×10^{-5}	37.0	1.74×10^{-3}	7.61×10^{-3}	3.54×10^{-4}
Arch Shaped Data	4.37×10^{-1}	1.18×10^{-4}	9.62×10^{-5}	37.2	1.46×10^{-2}	1.65×10^{-2}	1.75×10^{-2}

The Newton algorithm converges faster than the gradient algorithm, exploiting the second order information of the Hessian, as illustrated in Fig. 4 and Fig. 5. Although the Hessian computations are more complex, the Newton method takes only $5\,\mathrm{s}$ to converge to in a Matlab 7.3 implementation running on a standard computer with a Pentium Celeron 1.6 Ghz processor.

Defining the distance between the estimated and the actual parameter as $\mathbf{s}_e := \|\mathbf{S}^* - \mathbf{S}\|$,$\mathbf{b}_e := \|\mathbf{b}^* - \mathbf{b}\|$, and $\theta_e := \arccos\left(\frac{\mathrm{tr}(\mathcal{R}^*\mathcal{R}')-1}{2}\right)$, Tables I and II show that the arch shaped data set contains sufficient eccentricity information to estimate the equivalent magnetometer errors quantities $\mathcal{R}$, $\mathbf{s}$ and $\mathbf{b}$. For platforms with limited maneuverability, the proposed optimization algorithm identifies the calibration parameters with good accuracy. As expected, reducing the information about the ellipsoid curvature slightly degrades the sensor calibration errors.

As depicted in Fig. 3, although the noise is formulated in the sensor frame, the suboptimal formulation (10) yields accurate results with unitary likelihood weights $\sigma^2_{m\,i}$. Let the distance in the parameter space be given by $d(\mathbf{x}^*, \mathbf{x})^2 := \theta_e^2 + \mathbf{s}_e^2 + \mathbf{b}_e^2$, the influence of the noise power in the estimation error is illustrated in Fig. 6, where the magnetic field magnitude in the San Francisco Bay area is adopted, $\|^E\mathbf{h}\| = 0.5\,\mathrm{G}$.

B. Experimental Results

The algorithm proposed in this work was used to estimate the calibration parameters for a set of 6×10^4 points obtained from an actual magnetometer triad. The magnetometer was a Honeywell HMC1042L 2-axis magnetometer and a Honeywell HMC1041Z for the third (Z) axis, sampled with a TI MSC12xx microcontroller with a 24bit Delta Sigma converter, at 100Hz, see [10] for details.

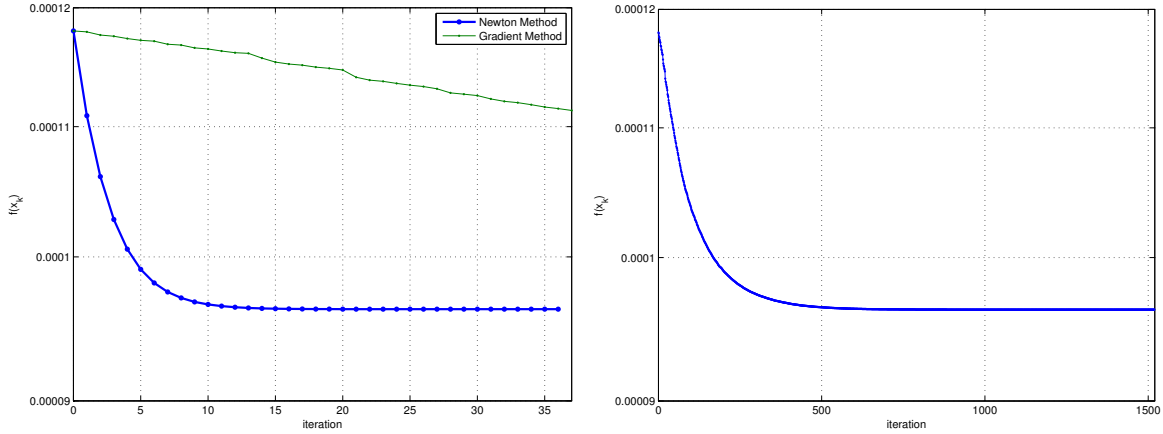

(a) Newton (vs Gradient) Method (b) Gradient Method Iterations

Fig. 4. Convergence of the Log-Likelihood Function (Arch Shaped Data)

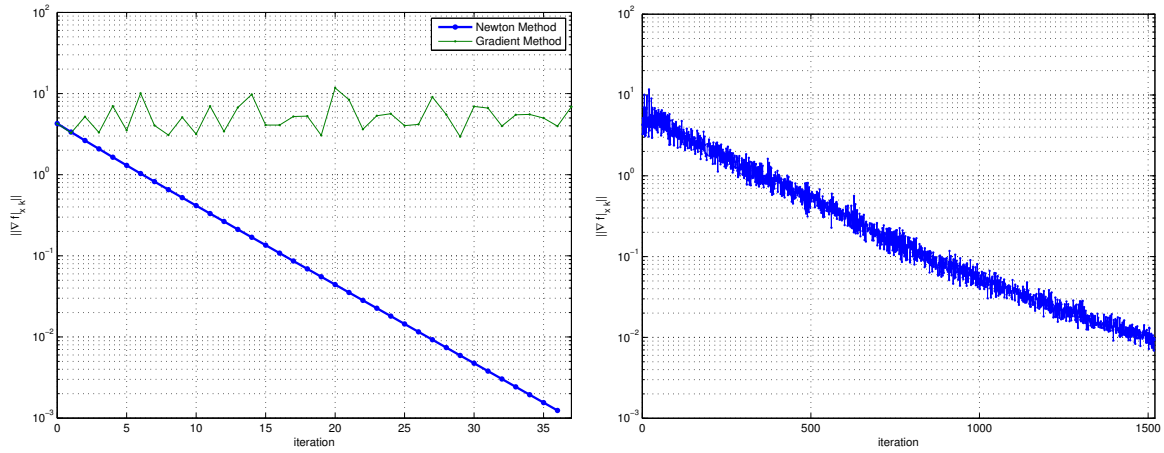

(a) Newton (vs Gradient) Method (b) Gradient Method Iterations

Fig. 5. Convergence of the Log-Likelihood Gradient (Arch Shaped Data)

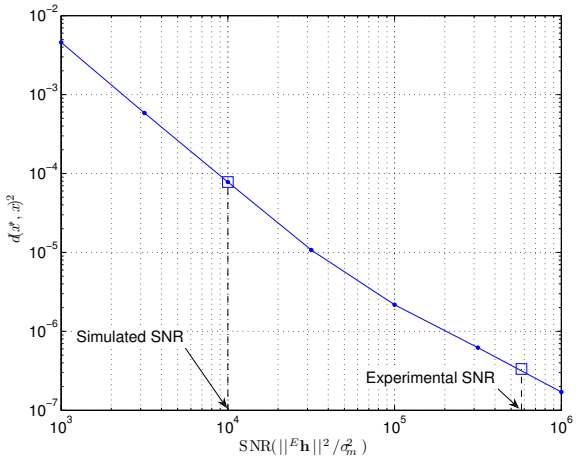

Fig. 6. Estimation Error vs. Signal-to-Noise Ratio (100 MC, Ring Shaped Data)

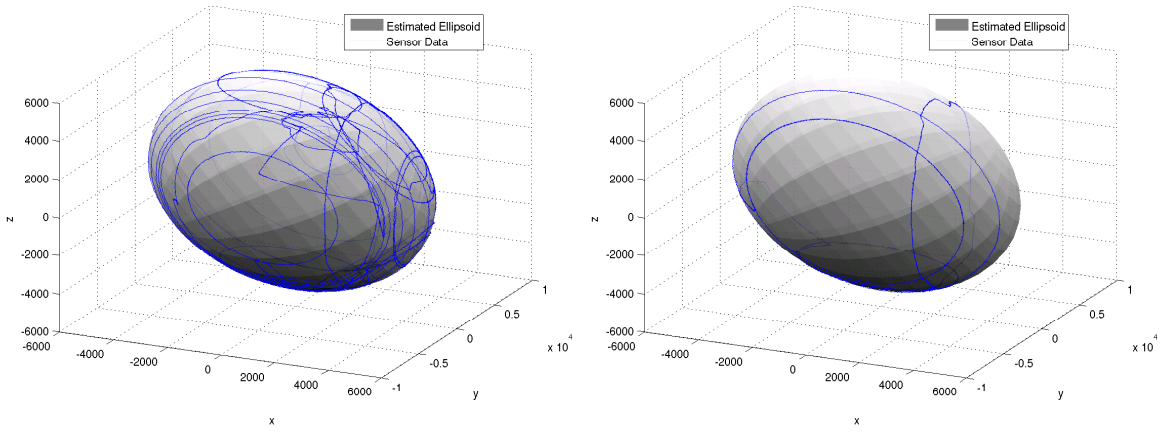

(a) Ellipsoid Surface Data (b) Ellipsoid Sections Data

Fig. 7. Ellipsoid Fitting (Real Data)

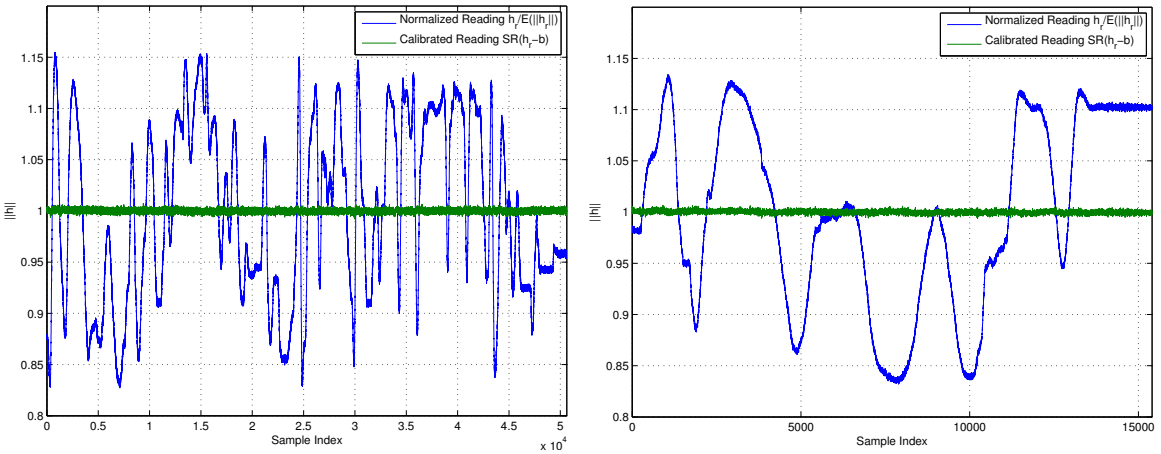

(a) Ellipsoid Surface Data (b) Ellipsoid Sections Data

Fig. 8. Magnetometer Data Fitting

A gimbal system was maneuvered to collect (i) a set of sensor readings spanning the ellipsoid surface, Fig. 7(a), (ii) only four ellipsoid sections, Fig. 7(b). The calibration algorithm converged to a minimum within 60 Newton method iterations, taking less than $40\,\mathrm{s}$ and yielding $f(\mathbf{x}^*) = 2.51 \times 10^{-6}$ for the ellipsoid surface data set and $f(\mathbf{x}^*) = 2.67 \times 10^{-6}$ for the ellipsoid sections data set. Although the second data set included less data points, the results were similar because the collected data were sufficient to characterize the ellipsoid's eccentricity and rotation, as depicted in Fig. 7(b).

Given the calibration parameters, the sensor noise is characterized by rewriting (7) as $\mathbf{n}_{m\,i} = \mathbf{h}_r - (\mathcal{R}_L^* \mathbf{S}_L^{*\,C}\mathbf{h}_i^* + \mathbf{b}^*)$ where ${}^C\mathbf{h}_i^*$ is given in the proof of Proposition 1. The obtained experimental standard deviation of the sensor noise is $\sigma_m = 0.65\,\mathrm{mG}$, which evidences that the signal-to-noise ratio of a typical low-cost magnetometer is better than that assumed in the simulations of Section III-A, as depicted in Fig. 6.

The calibrated magnetometer data are compared to the raw data in Fig. 8. The calibrated readings are near to the unit circle locus, which validates the proposed unified error formulation of Theorem 1 and shows that the combined effect of the magnetic distortions is successfully compensated for.

IV. Conclusions

A new estimation algorithm was derived and successfully validated for the onboard calibration of three-axis strapdown magnetometers. After a detailed characterization on the disturbances corrupting the magnetometer readings, an equivalent error parametrization was derived. The magnetometer calibration was shown to be equivalent to the estimation of an ellipsoid manifold. The parameter optimization problem was formulated resorting to a Maximum Likelihood Estimator, and an optimization algorithm was derived using the gradient and Newton descent methods. A closed form solution for the magnetometer alignment was obtained from the solution to the orthogonal Procrustes problem. The performance of the proposed methodology was assessed both in simulation and with experimental data from low-cost sensors. Results show that the proposed calibration

algorithm can be adopted for a wide variety of autonomous vehicles with maneuverability constraints and in situations that require periodic onboard sensor calibration. Future work will include the adaptation of the proposed algorithm to the 2D (heading only) case in marine and land robotics.

EXTERNAL MAGNETIC NOISE

In the proposed error model (4), electronic interference and sensor specific technology are the main sources of noise. In the case where the main sources of electromagnetic interference are external, the magnetic noise influence in the magnetometer reading can be modeled as

$$\begin{aligned}\mathbf{h}_{r\,i} &= \mathbf{S}_M\mathbf{C}_{NO}(\mathbf{C}_{SI}({}^B_E\mathbf{R}_i{}^E\mathbf{h} + {}^B_N\mathbf{R}\,\mathbf{n}_{m\,i}) + \mathbf{b}_{HI}) + \mathbf{b}_M = \mathbf{C}^B\mathbf{h}_i + \mathbf{C}^B_N\mathbf{R}\,\mathbf{n}_{m\,i} + \mathbf{b} \\ &= \mathcal{R}_L\mathbf{S}_L{}^C\mathbf{h}_i + \mathcal{R}_L\mathbf{S}_L\mathbf{V}'_L{}^B_N\mathbf{R}\,\mathbf{n}_{m\,i} + \mathbf{b} \end{aligned} \tag{16}$$

where ${}^B_N\mathbf{R}$ rotates from the coordinate frame $\{N\}$ where the magnetic noise is defined, to the body coordinate frame. Assuming that $\mathbf{n}_{m\,i}$ is a zero mean Gaussian process with variance $\sigma^2_{m\,i}$, the p.d.f. of each $\mathbf{h}_{r\,i}$ is also Gaussian

$$\mathbf{n}_{m\,i} \sim \mathcal{N}(0, \sigma^2_{m\,i}\mathbf{I}) \Rightarrow \mathbf{h}_{r\,i} \sim \mathcal{N}(\mathcal{R}_L\mathbf{S}_L{}^C\mathbf{h}_i + \mathbf{b}, \sigma^2_{m\,i}\mathcal{R}_L\mathbf{S}^2_L\mathcal{R}'_L).$$

Using the p.d.f. of the $\mathbf{h}_{r\,i}$, straightforward analytical derivations show that MLE formulation is given by (9). As convincingly argued in [22], if the noise exists in the sensor frame (7), the ellipsoid obtained by (9) tends to fit best the points with lower eccentricity. This effect can be balanced by defining appropriate curvature weights [22] $\sigma^2_{m\,i}$, producing results close to the optimal solution of (8).

LIKELIHOOD FUNCTION DERIVATIVES

Let $\mathbf{u}_i := \mathbf{h}_{r\,i} - \mathbf{b}$, the gradient of the likelihood function

$$f := \sum_{i=1}^{n}\left(\frac{\|\mathbf{T}(\mathbf{h}_{r\,i} - \mathbf{b})\| - 1}{\sigma_{m\,i}}\right)^2,$$

denoted by $\nabla f|_{\mathbf{x}} = \begin{bmatrix}\nabla f|_{\mathbf{T}} & \nabla f|_{\mathbf{b}}\end{bmatrix}$, is described by the submatrices

$$\nabla f|_{\mathbf{T}} = \sum_{i=1}^{n}\frac{2c_T}{\sigma^2_{m\,i}}\mathbf{u}_i \otimes \mathbf{T}\mathbf{u}_i, \qquad \nabla f|_{\mathbf{b}} = \sum_{i=1}^{n}\frac{-2c_T}{\sigma^2_{m\,i}}\mathbf{T}'\mathbf{T}\mathbf{u}_i,$$

where $c_T := 1 - \|\mathbf{T}\mathbf{u}_i\|^{-1}$ and $\otimes$ denotes the Kronecker product [23]. The Hessian $\nabla^2 f|_{\mathbf{x}} = \begin{bmatrix}\mathbf{H}_{\mathbf{T},\mathbf{T}} & \mathbf{H}_{\mathbf{T},\mathbf{b}} \\ \mathbf{H}'_{\mathbf{T},\mathbf{b}} & \mathbf{H}_{\mathbf{b},\mathbf{b}}\end{bmatrix}$ is given by the following submatrices

$$\mathbf{H}_{\mathbf{T},\mathbf{T}} = \sum_{i=1}^{n}\frac{2}{\sigma^2_{m\,i}}\left[\frac{(\mathbf{u}_i\mathbf{u}'_i)\otimes(\mathbf{T}\mathbf{u}_i\mathbf{u}'_i\mathbf{T}')}{\|\mathbf{T}\mathbf{u}_i\|^3} + c_T\left[(\mathbf{u}_i\mathbf{u}'_i)\otimes\mathbf{I}\right]\right], \quad \mathbf{H}_{\mathbf{T},\mathbf{b}} = \sum_{i=1}^{n}\frac{-2}{\sigma^2_{m\,i}}\left[\frac{(\mathbf{u}_i\otimes\mathbf{T}\mathbf{u}_i)\,\mathbf{u}'_i\mathbf{T}'\mathbf{T}}{\|\mathbf{T}\mathbf{u}_i\|^3} + c_T\left(\mathbf{u}_i\otimes\mathbf{T} + \mathbf{I}\otimes\mathbf{T}\mathbf{u}_i\right)\right]$$

$$\mathbf{H}_{\mathbf{b},\mathbf{b}} = \sum_{i=1}^{n}\frac{2}{\sigma^2_{m\,i}}\left[\frac{\mathbf{T}'\mathbf{T}\mathbf{u}_i\mathbf{u}'_i\mathbf{T}'\mathbf{T}}{\|\mathbf{T}\mathbf{u}_i\|^3} + c_T\mathbf{T}'\mathbf{T}\right].$$

ACKNOWLEDGMENTS

This work was partially supported by Fundação para a Ciência e a Tecnologia (ISR/IST plurianual funding) through the POS_Conhecimento Program that includes FEDER funds and by the project MEDIRES from ADI and project PDCT/MAR/55609/2004 - RUMOS of the FCT. The work of J.F. Vasconcelos was supported by a PhD Student Scholarship, SFRH/BD/18954/2004, from the Portuguese FCT POCTI programme.

REFERENCES

[1] T. E. Humphreys, M. L. Psiaki, E. M. Klatt, S. P. Powell, and P. M. Kintner, Jr., "Magnetometer-based attitude and rate estimation for spacecraft with wire booms," *Journal of Guidance, Control, and Dynamics*, vol. 28, no. 4, pp. 584–593, July-August 2005.

[2] D. Choukroun, I. Y. Bar-Itzhack, and Y. Oshman, "Optimal-request algorithm for attitude determination," *Journal of Guidance, Control, and Dynamics*, vol. 27, no. 3, pp. 418–425, May-June 2004.

[3] I. Bar-Itzhack and R. Harman, "Optimized TRIAD Algorithm for Attitude Determination," *Journal of Guidance, Control, and Dynamics*, vol. 20, no. 1, pp. 208–211, 1997.

[4] D. M. F. L. Markley, "Quaternion attitude estimation using vector observations," *Journal of Astronautical Sciences*, vol. 48, no. 2, pp. 359–380, 2000.

[5] *NOAA Technical Report: The US/UK World Magnetic Model for 2005-2010*, National Oceanic and Atmospheric Administration, U.S. Department of Commerce, 2004.

[6] F. Markley, "Attitude determination and parameter estimation using vector observations: Theory," *The Journal of the Astronautical Sciences*, vol. 37, no. 1, pp. 41–58, January-March 1989.

[7] W. Denne, *Magnetic Compass Deviation and Correction*, 3rd ed. Sheridan House Inc, 1979.

[8] N. Bowditch, *The American Pratical Navigator*, Hydrographic/Topographic Center, Defense Mapping Agency, 1984.

[9] D. Gebre-Egziabher, G. Elkaim, J. Powell, and B. Parkinson, "Calibration of Strapdown Magnetometers in Magnetic Field Domain," *ASCE Journal of Aerospace Engineering*, vol. 19, no. 2, pp. 1–16, April 2006.

[10] G. Elkaim and C. Foster, "Development of the metasensor: A low-cost attitude heading reference system for use in autonomous vehicles," in *Proceedings of the ION Global Navigation Satellite Systems Conference (ION-GNSS 2006)*, Fort Worth, TX, USA, September 2006.

[11] R. Alonso and M. Shuster, "Complete linear attitude-independent magnetometer calibration," *The Journal of the Astronautical Sciences*, vol. 50, no. 4, pp. 477–490, October-December 2002.

[12] B. Gambhir, "Determination of Magnetometer Biases Using Module RESIDG," Computer Sciences Corporation, Tech. Rep. 3000-32700-01TN, March 1975.

[13] J. Crassidis, K. Lai, and R. Harman, "Real-time attitude-independent three-axis magnetometer calibration," *Journal of Guidance, Control, and Dynamics*, vol. 28, no. 1, pp. 115–120, January-February 2005.

[14] J. C. Gower and G. B. Dijksterhuis, *Procrustes Problems*, ser. Oxford Statistical Science Series. Oxford University Press, USA, 2004, no. 30.

[15] G. Elkaim and C. Foster, "Extension of a Non-Linear, Two-Step Calibration Methodology to Include Non-Orthogonal Sensor Axes," 2006, iEEE Journal of Aerospace Electronic Systems, Technical Note, submitted August 2006, accepted for publication.

[16] G. Strang, *Linear Algebra and Its Applications*, 3rd ed. Brooks Cole, 1988.

[17] A. Edelman, T. Arias, and S. Smith, "The geometry of algorithms with orthogonality constraints," *SIAM Journal on Matrix Analysis and Applications*, vol. 20, no. 2, pp. 303–353, 1998.

[18] D. Gabay, "Minimizing a differentiable function over a differential manifold," *Journal of Optimization Theory and Applications*, vol. 37, no. 2, pp. 177–219, June 1982, communicated by D.G. Luenberger.

[19] S. Kay, *Fundamentals of Statistical Signal Processing: Estimation*. Upper Saddle River, New Jersey, USA: Prentice-Hall, 1993.

[20] D. Bertsekas, *Nonlinear Programming*, 2nd ed. Athena Scientific, 1999.

[21] G. Calafiore, "Approximation of n-dimensional data using spherical and ellipsoidal primitives," *IEEE Transactions on Systems, Man and Cybernetics - Part A: Systems and Humans*, vol. 32, no. 2, pp. 269–278, March 2002.

[22] W. Gander, G. Golub, and R. Strebel, "Least-squares fitting of circles and ellipses," *BIT*, vol. 43, pp. 558–578, 1994.

[23] H. Lütkepohl, *Handbook of Matrices*. John Wiley & Sons, 1997.